



This is a repository copy of *Effective thermal conductivity of porous solder layers* .

White Rose Research Online URL for this paper:
<http://eprints.whiterose.ac.uk/856/>

Article:

Pritchard, L.S., Acarnley, P.P. and Johnson, C.M. (2004) Effective thermal conductivity of porous solder layers. *IEEE Transactions on Components and Packaging Technologies*, 27 (2). pp. 259-267. ISSN 1521-3331

<https://doi.org/10.1109/TCAPT.2004.828584>

Reuse

Unless indicated otherwise, fulltext items are protected by copyright with all rights reserved. The copyright exception in section 29 of the Copyright, Designs and Patents Act 1988 allows the making of a single copy solely for the purpose of non-commercial research or private study within the limits of fair dealing. The publisher or other rights-holder may allow further reproduction and re-use of this version - refer to the White Rose Research Online record for this item. Where records identify the publisher as the copyright holder, users can verify any specific terms of use on the publisher's website.

Takedown

If you consider content in White Rose Research Online to be in breach of UK law, please notify us by emailing eprints@whiterose.ac.uk including the URL of the record and the reason for the withdrawal request.



eprints@whiterose.ac.uk
<https://eprints.whiterose.ac.uk/>

Effective Thermal Conductivity of Porous Solder Layers

Leonard S. Pritchard, Paul P. Acarnley, and C. Mark Johnson, *Member, IEEE*

Abstract—Microscopic voids in the die attachment solder layers of power semiconductor devices degrade their overall thermal transfer performance. This paper presents analytical results of the effect of spherical and spheroidal void geometries on the thermal conductivity of bulk media. Analytical results are compared with axially symmetric and three-dimensional thermal simulations of single and multiple cavity defects in planar structures. The effective thermal conductivity of the die to case attachment solder layer of two commercial metal oxide semiconductor field effect transistor (MOSFET) devices is estimated using these results, with cavity dimensions and distributions obtained by electron microscopy.

Index Terms—Analytical model, die attach, finite element simulation, MOSFET, packaging, power semiconductor, solder layers, thermal conductivity, voids.

I. INTRODUCTION

POWER semiconductor devices have at least one internal solder layer, namely that attaching the die to the package metal base plate, as illustrated in Fig. 1.

A further solder layer is used in those devices where the die is electrically isolated from the case with a thin dielectric plate. Although the solder layers are thin, the alloys used have comparatively low thermal conductivities, and can produce significant thermal resistances in these regions [1], [2].

Electron microscopy was used to investigate the solder layer of a sample of commercial power MOSFET devices. Substantial variation in the solder thickness was measured between devices, in the approximate range 10–50 μm . In addition, internal voids of various sizes and distributions were observed. Some layers had relatively large cavities, but few in number. By contrast, other solder layers contained many more voids of smaller dimensions [2]. Internal voids must reduce the overall thermal conductivity to some degree, the extent of which forms the subject matter of this paper.

Various techniques have been used to model the effect, especially for multiple cavity systems, including volume averaging [3], analogy with micro-cracks in elastic solids [4] and sum-



Fig. 1. Cross sectional schematic of a power semiconductor device.

mation of thermal resistance components [5]. The method presented here is based on a field analysis.

To obtain analytical solutions for the reduced heat flow, the effects of regular cavity geometries are considered. Spherical and spheroidal (oblate and prolate) bodies are introduced into a base material supporting an otherwise uniform, steady-state thermal field. Expressions for the disturbance to the heat flow path are used to derive effective thermal conductivities for the various inclusion geometries. The analytical results are compared with finite element thermal simulations for single cavities of various sizes in a cylindrical system. Simulations are also performed to evaluate the accuracy of the analysis to systems with multiple spherical cavities. These simulations used randomly placed cavities with separations to minimize field interactions.

Estimates of the effective thermal conductivity of two MOSFET die attachment solder layers are calculated. These estimates use the analytical results for spherical cavities with approximate cavity dimensions and number densities measured from the electron micrographs.

II. THERMAL ANALYSIS

A three-dimensional (3-D) steady-state thermal field, without heat sources or sinks is described by Laplace's equation [6]

$$\frac{\partial^2 T}{\partial x^2} + \frac{\partial^2 T}{\partial y^2} + \frac{\partial^2 T}{\partial z^2} = 0$$

or

$$\nabla^2 T = 0. \quad (1)$$

The rate of heat flow per unit area \mathbf{q} is described by Fourier's law, where σ_{th} is the thermal conductivity

$$\mathbf{q} = -\sigma_{th} \nabla T. \quad (2)$$

The thermal field, \underline{p} , is defined by

$$\underline{p} \equiv -\nabla T.$$

The following general property of Laplacian fields is used in the derivations of effective thermal conductivity. Consider a volume, V_T , initially of uniform thermal conductivity σ_o , into which a cavity of conductivity σ_c and volume V_c , is introduced. Fig. 2 illustrates the situation before and after introduction of

Manuscript received May 1, 2003; revised August 6, 2003. This work was supported by UK Engineering and Physical Sciences Research Council (EPSRC) Research Grant GR/R02634/01. This work was recommended for publication by Associate Editor K. C. Toh upon evaluation of the reviewers' comments.

L. S. Pritchard and P. P. Acarnley are with the Department of Electrical, Electronic and Computer Engineering, University of Newcastle upon Tyne, Newcastle upon Tyne NE1 7RU, U.K.

C. M. Johnson is with the Electrical Machines and Drives Research Group, University of Sheffield, Sheffield S1 3JD, U.K. (e-mail: c.m.johnson@sheffield.ac.uk).

Digital Object Identifier 10.1109/TCAPT.2004.828584

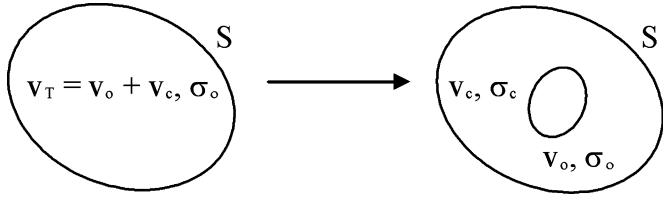


Fig. 2. Change in field quantities after the introduction of a cavity with different thermal conductivity.

the cavity. Note that v_o is the volume enclosed by surface S minus the cavity. The temperature and heat flow distributions change from T_1 to T_2 and \mathbf{q}_1 to \mathbf{q}_2 , respectively.

Assume that $T_1 = T_2$ on the surface S .

The change in the volume integral

$$\int_{v_T} \mathbf{p} \cdot \mathbf{q} dv$$

can be expressed as

$$\int_{v_T} (\mathbf{p}_1 \cdot \mathbf{q}_1 - \mathbf{p}_2 \cdot \mathbf{q}_2) dv = \int_{v_c} (\sigma_o - \sigma_c) \mathbf{p}_1 \cdot \mathbf{p}_2 dv \quad (3)$$

where $v_T = v_o + v_c$.

Since $\mathbf{q}_1 = \sigma_o \mathbf{p}_1$ over the whole volume, (3) becomes [see Appendix A]

$$\int_{v_T} \sigma_o \mathbf{p}_1^2 dv - \int_{v_T} \mathbf{p}_2 \cdot \mathbf{q}_2 dv = \int_{v_c} (\sigma_o - \sigma_c) \mathbf{p}_1 \cdot \mathbf{p}_2 dv$$

or

$$\sigma_{\text{EFF}} \equiv \frac{\int_{v_T} \mathbf{p}_2 \cdot \mathbf{q}_2 dv}{\int_{v_T} \mathbf{p}_1^2 dv} = \sigma_o - \frac{\int_{v_c} (\sigma_o - \sigma_c) \mathbf{p}_1 \cdot \mathbf{p}_2 dv}{\int_{v_T} \mathbf{p}_1^2 dv} \quad (4)$$

Equation (4) defines an effective thermal conductivity, σ_{EFF} over the volume v_T , expressible in terms of the initial undisturbed field and the modified field inside v_c .

The various cavity geometries are considered in turn.

Fig. 3 shows the general case of an ellipsoid of thermal conductivity σ_c placed in a region of uniform thermal field \mathbf{p}_1 and conductivity σ , in this case with $\sigma_c < \sigma$. The two views are along the orthogonal axes "c" and "b," respectively, with the field parallel to the "a" axis.

The field inside the cavity is uniform and parallel to the ambient field, as expressed by (5) [see Appendix B]

$$\mathbf{p}_2 = \frac{\mathbf{p}_1}{\left(1 + \frac{abc}{2\sigma} [\sigma_c - \sigma] A_1\right)} \quad (5)$$

where

$$A_1 = \int_0^\infty \frac{du}{\left([u + a^2]^3 [u + b^2] [u + c^2]\right)^{\frac{1}{2}}} \quad (6)$$

and u is a parameter representing a family of ellipsoidal surfaces.

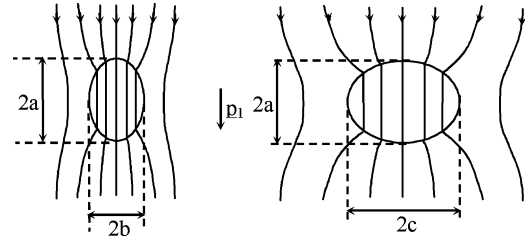


Fig. 3. Thermal field distortion by an ellipsoidal inclusion in a uniform field.

A. Spherical Cavity

For a spherical cavity, $a = b = c = \text{radius } R$ and

$$A_1 = \int_0^\infty \frac{du}{(u + R^2)^{\frac{5}{2}}} = \frac{2}{3R^3}.$$

Giving

$$\mathbf{p}_2 = \frac{3\sigma}{(2\sigma + \sigma_c)} \cdot \mathbf{p}_1. \quad (7)$$

Using (4)

$$\sigma_{\text{EFF}} = \sigma \left(1 - 3 \left[\frac{\sigma - \sigma_c}{2\sigma + \sigma_c}\right] \cdot \frac{v_c}{v_T}\right). \quad (8)$$

For a vacuum cavity with $\sigma_c = 0$ and neglecting radiation exchange of heat

$$\sigma_{\text{EFF}} = \sigma \left(1 - \frac{3}{2} \cdot \frac{v_c}{v_T}\right). \quad (9)$$

B. Oblate Spheroidal Cavity

An oblate spheroidal cavity has $b = c$ with $a < c$. This geometry can be used to estimate the effect of delamination type defects by setting $a \ll c$, for example

$$A_1 = \int_0^\infty \frac{du}{[u + a^2]^{\frac{3}{2}} [u + c^2]}.$$

Giving

$$A_1 = \frac{2}{[c^2 - a^2]^{\frac{3}{2}}} \left(\frac{[c^2 - a^2]^{\frac{1}{2}}}{a} - \arctan \frac{[c^2 - a^2]^{\frac{1}{2}}}{a} \right). \quad (10)$$

Equation (5) becomes

$$\mathbf{p}_2 = \frac{\mathbf{p}_1}{\left(1 + \frac{ac^2}{2\sigma} [\sigma_c - \sigma] A_1\right)}. \quad (11)$$

In (4)

$$\sigma_{\text{EFF}} = \sigma \left(1 - \frac{[\sigma - \sigma_c]}{\left(\sigma + \frac{ac^2}{2} [\sigma_c - \sigma] A_1\right)} \cdot \frac{v_c}{v_T}\right). \quad (12)$$

When $\sigma_c = 0$

$$\sigma_{\text{EFF}} = \sigma \left(1 - \frac{1}{\left(1 - \frac{ac^2}{2} A_1\right)} \cdot \frac{v_c}{v_T}\right). \quad (13)$$

C. Prolate Spheroidal Cavity

A prolate spheroidal cavity has $b = c$ and $a > c$. In this case, the geometry is 'stretched' in the direction of the field and could

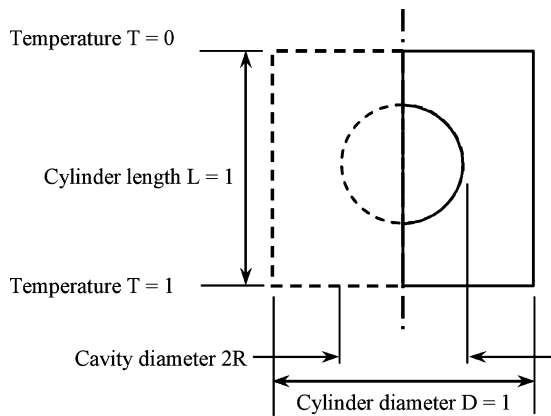


Fig. 4. Geometry of the axially symmetric system used in the simulations.

be used for estimating the effects of fissure type defects, for example. With $a > c$, (10) becomes

$$A_1 = \frac{2}{[a^2 - c^2]^{\frac{3}{2}}} \left(\frac{1}{2} \ln \left[\frac{1+e}{1-e} \right] - e \right) \quad (14)$$

where

$$e = \frac{(a^2 - c^2)^{\frac{1}{2}}}{a}$$

this expression is used in (12) and (13) to calculate the effective conductivity, σ_{EFF} .

III. SIMULATIONS

Simulations were performed for the various cavity geometries using a commercial finite element program [8]. In this way, a comparison of the results of the preceding section could be made with those for planar systems with imposed boundary conditions. For single cavities, axially symmetric analyzes were performed to reduce solution times and memory requirements. These simulations modeled cylindrical systems of unit diameter and length, with almost zero thermal conductivity set for the cavity and unit conductivity for the surrounding medium. Unit thermal gradient was established by setting the lower face of the cylinder to unit temperature and the upper face to zero.

A. Spherical Cavity

A number of simulations were performed using a range of cavity diameters from 0.1 unit to 0.8, placed centrally in a unit dimension cylinder, as illustrated in Fig. 4. Fig. 5 shows the simulation results with the heat flow path for cavity diameters at the extremes of the range. The arrow lengths represent the magnitude of the heat flux per unit area, calculated at the finite element centroids.

These simulations enabled the total heat flow through the cylinder to be calculated by summing the heat flux results at the upper (or lower) surface, from which the effective thermal conductivity was evaluated. Fig. 6 is a graph plotting effective conductivity against relative cavity diameter compared with the values calculated from (9).

Simulations were also performed to investigate the effect of axial offset in the cavity position. For a 0.2 unit diameter spher-

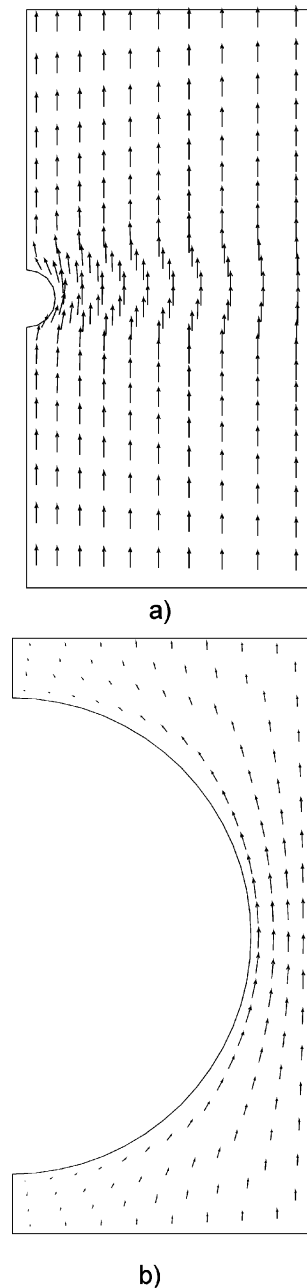


Fig. 5. Heat flow path for 0.1 and 0.8 diameter cavities.

ical cavity, the difference in effective thermal conductivity between a cavity with a central location and one with the cavity centre $3/4$ from the base (or top) is approximately 0.01%. For a 0.4 diameter cavity, the corresponding difference is approximately 0.2%.

Equation (9) relates the reduction in thermal conductivity to a function of the cavity to system volume ratio. It is reasonable to expect that multiple cavities, sufficiently separated to minimize field interaction, will produce a net effect that can be calculated from the total cavity to system volume ratio. To investigate further, 3-D analyses were made with increasing numbers of 0.2 diameter spherical cavities in a unit cube. The cavities were distributed over the full cube volume, but positioned to avoid overlap or close proximity. Fig. 7 plots the results of the simulations for comparison with (9) using the total cavity volume.

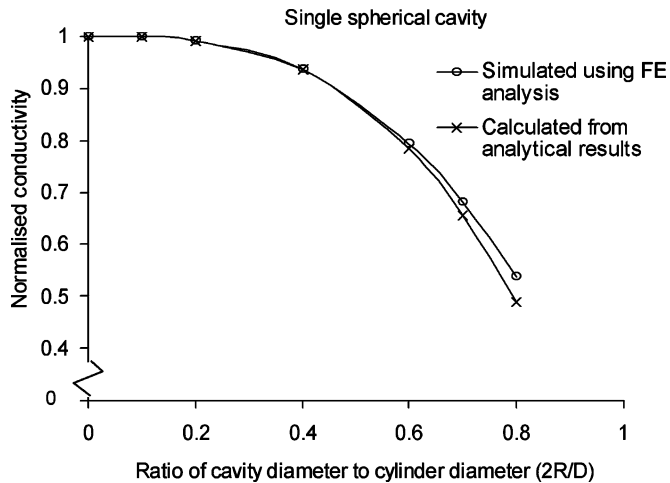


Fig. 6. Graph of effective thermal conductivity as a function of relative cavity diameter.

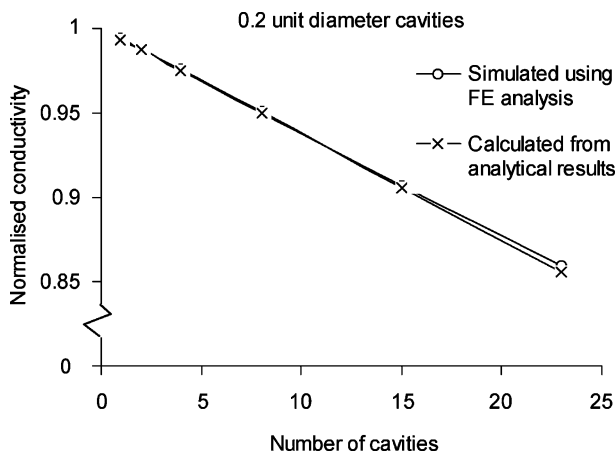


Fig. 7. Effective thermal conductivity with number of 0.2 diameter cavities in a unit cube.

The results are in close agreement up to the maximum of 23 cavities considered, although the effect of increasing total cavity to system volume ratio, discussed in Section V, must be taken into account.

B. Oblate Spheroidal Cavity

Fig. 8 shows the position of the oblate cavity in a unit cylinder. Heat flow paths for cavities with $c = 0.45$ and axis ratios $a/c = 0.1$ and 0.05 respectively are presented in Fig. 9, while Fig. 10 is an expanded view of the outlined region in Fig. 9 showing detail of the heat flow at the edge of the cavity. Figs. 11 and 12 show the effective thermal conductivity for a range of values for axis c , comparing simulation results with calculations from (13) and (10). The axis ratios are $a/c = 0.1$ and 0.05 , respectively.

The largest cavity, with a diameter to cylinder diameter ratio of 0.9, covers approximately 0.8 of the cylinder cross sectional area. In this case, a smaller figure for effective conductivity might be expected. However a large temperature gradient develops between the edge of the cavity and the cylinder surface that produces a high rate of heat flow in this region, as evident in Fig. 10.

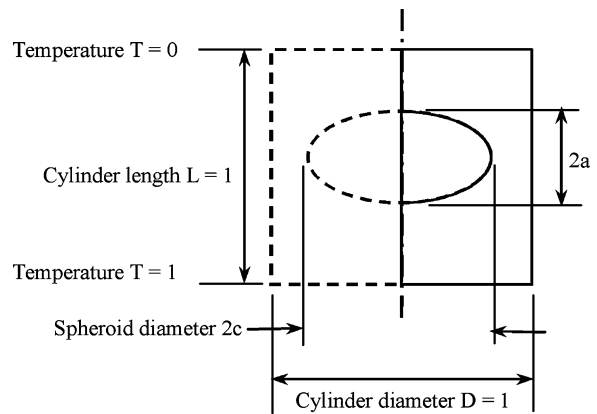


Fig. 8. Geometry of oblate spheroidal cavity in unit cylinder.

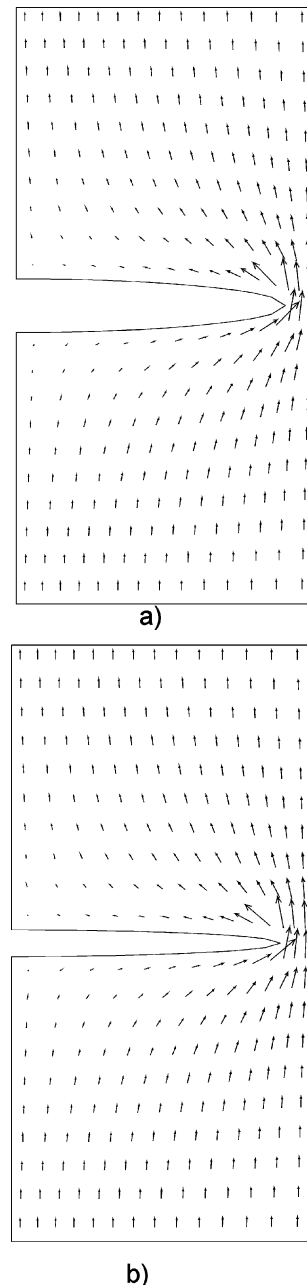


Fig. 9. Heat flow paths for oblate spheroidal cavities of semi-axis $c = 0.45$ and axis ratio 0.1 and 0.05, respectively.

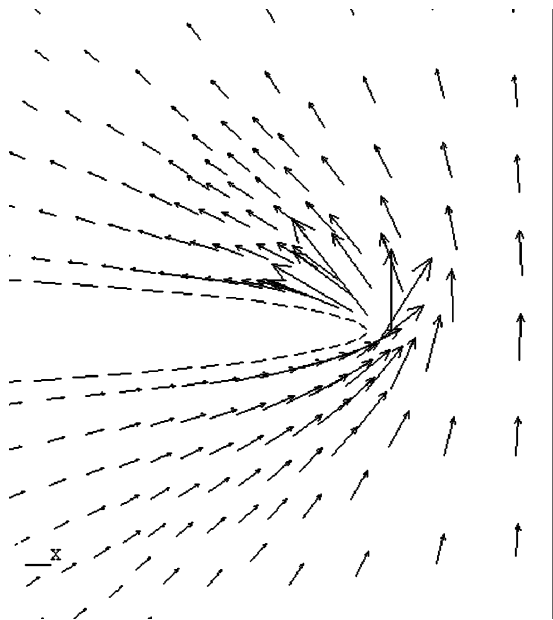


Fig. 10. Expanded view of the heat flow path around the edge of the cavity of axis ratio 0.05.

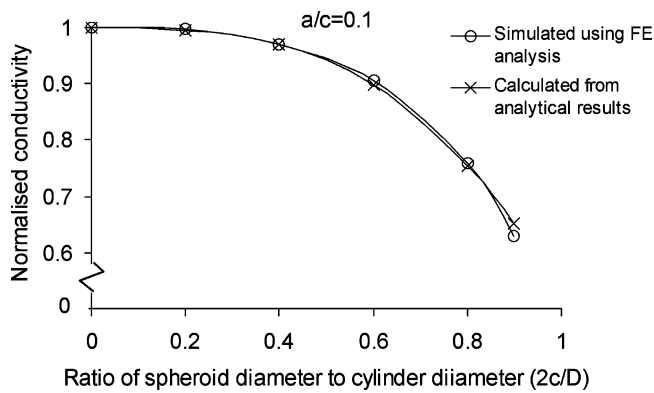


Fig. 11. Effective thermal conductivity of an oblate spheroid as a function of spheroid diameter for axis ratio $a/c = 0.1$.

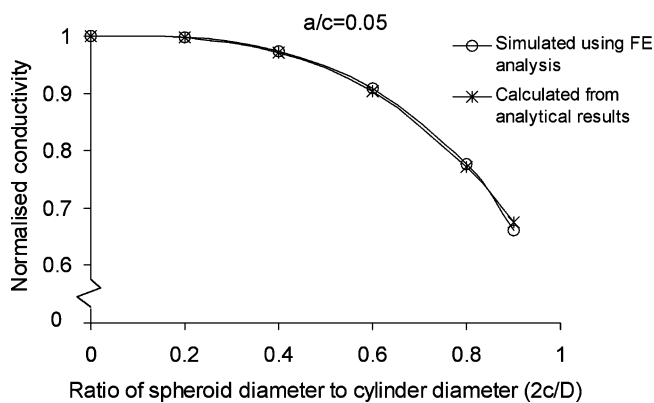


Fig. 12. Effective thermal conductivity of an oblate spheroid as a function of spheroid diameter for axis ratio $a/c = 0.05$.

C. Prolate Spheroidal Cavity

Fig. 13 shows the prolate geometry in a unit cylinder and Fig. 14 presents the simulation heat flow results for a cavity with $c = 0.045$ and axis ratio $a/c = 10$. Fig. 15 is an expanded view

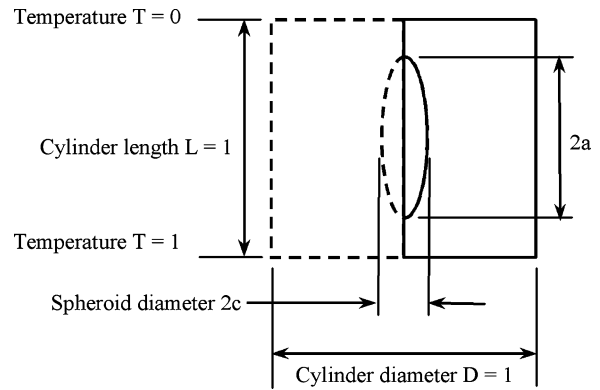


Fig. 13. Geometry of prolate spheroidal cavity in unit cylinder.

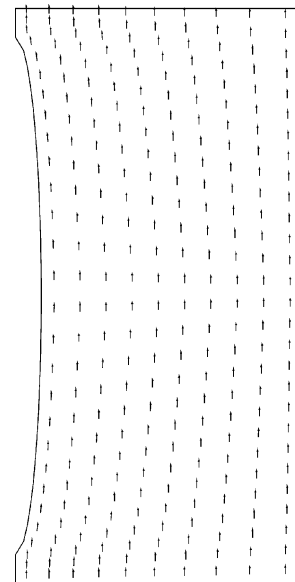


Fig. 14. Heat flow paths for prolate spheroidal cavity of semi-axis $c = 0.045$ and axis ratio 10.

of the indicated region at the top of the cavity whilst Fig. 16 compares the calculations from (13) with (14) with simulation results for a range of cavity dimensions and an axis ratio $a/c = 10$.

The reduction in heat flow from these cavities is much less than the oblate case, caused by lower values of A_1 (14). In addition, cavity volume is much reduced for small spheroid diameters, with $v_c = 4\pi c^2 a/3$. For example, an oblate cavity with $a = 0.045$ and axis ratio $a/c = 0.1$ has a volume of 3.82×10^{-2} , this may be compared with a prolate cavity of $a = 0.45$ and $a/c = 10$ whose volume is an order of magnitude smaller.

IV. SOLDER LAYERS

A total of nine devices, three from each of three different manufacturers, were cut up for examination by electron microscopy. These devices were commercial power switching MOSFETS in TO-220 plastic packages and of the same type designation. Fig. 17 shows the position of the cut plane and viewing direction and Fig. 18 is a typical low magnification image ($\times 35$) showing the overall structure.

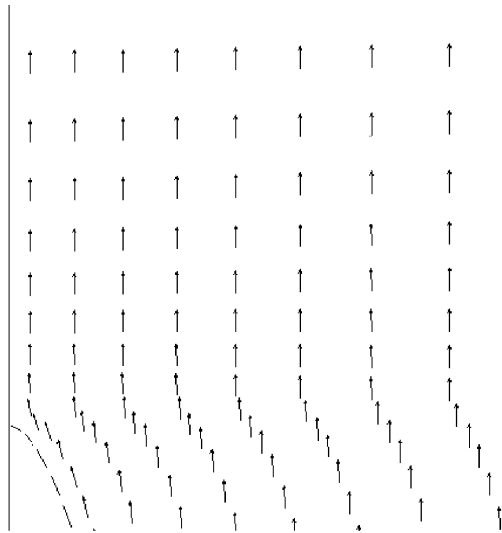


Fig. 15. Expanded view of the heat flow path at the top of the prolate cavity.

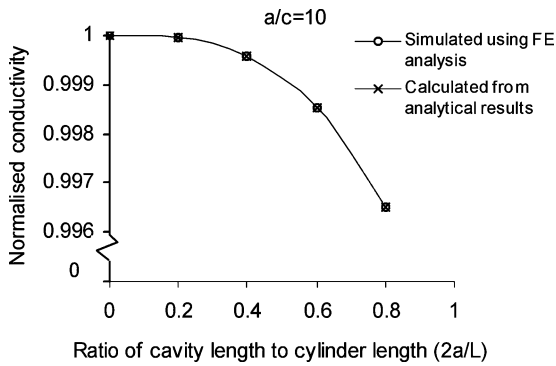


Fig. 16. Effective thermal conductivity of a prolate spheroid as a function of spheroid length for axis ratio $a/c = 10$.

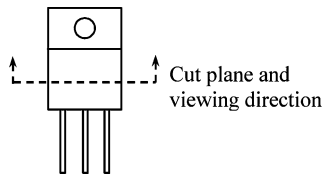


Fig. 17. Direction of cut plane and the viewing direction for electron microscopy.

At $\times 1000$ magnification, the solder layer became clearly visible, and imaging with back scattered electrons was chosen to reveal cavities. All of the devices were examined; the two with the greatest degree of solder voiding are shown in Fig. 19.

From these images, the cavities were counted according to the numbers falling into discrete ranges of approximate diameter. In this way, an area density for each diameter range was estimated, in turn converted to volume densities by raising to the power $3/2$. Assuming the voids to be spherical, the volume densities were used to estimate the total cavity to solder volume for each device.

For device (a), the volume fraction $v_c/v_T \sim 1.2 \times 10^{-3}$ and assuming negligible heat transfer within the cavities, $\sigma_c = 0$, (9) gives

$$\frac{\sigma_{EFF}}{\sigma} \approx 0.99.$$

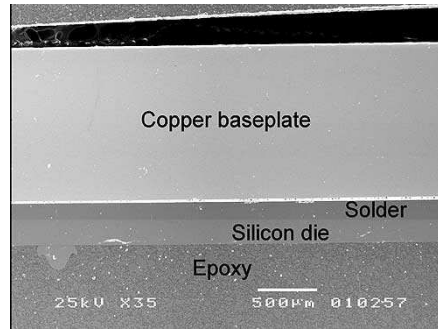


Fig. 18. Cross section through a power MOSFET at $\times 35$ magnification.

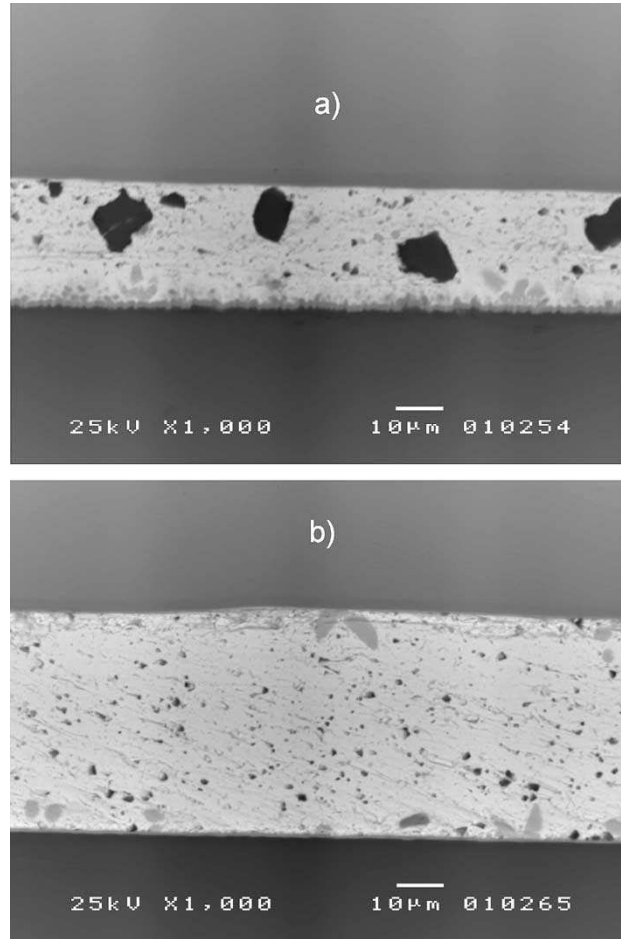


Fig. 19. Images at $\times 1000$ magnification revealing cavities within the solder layer of two devices.

For device (b), the volume fraction $v_c/v_T \sim 0.0316$ and

$$\frac{\sigma_{EFF}}{\sigma} \approx 0.95.$$

These figures are based on the single cross-sectional micrographs of the solder layers.

V. DISCUSSION

Differences between simulated and calculated effective thermal conductivity are generally low for small cavities. For example, with spherical geometry the difference is $< 0.1\%$ up to a cavity to cylinder diameter ratio of almost 0.4. Beyond this point, the difference increases more rapidly until it reaches

approximately 9% at a ratio of 0.8. The derivations of Section II assume that the cavities are in a uniform field, unaffected by the introduction of the void. With the simulations, the background thermal field is produced by a finite cylindrical system with constant temperature boundary conditions at the top and bottom surfaces and zero radial heat flow through the cylindrical surface. Clearly, the two systems are not the same, and they produce solutions that progressively diverge as the ratio of cavity to cylinder volume increases, when the cavity surface approaches the bounding surfaces. Test simulations for a spherical void show that the internal field is markedly nonuniform for large volume ratios, with significant deviations from (7). Similarly, the simple summation of cavity volume in situations of multiple voiding assumes that the cavities are sufficiently separated that the field disturbances do not significantly interact.

The calculation of thermal conductivity reduction factors for the solder layers of the two MOSFET devices assumes spherical voiding. When spherical, and ellipsoidal cavities in general, are placed in a uniform field, the internal field is also uniform. This result simplifies the formulation of effective conductivity for these geometries. However, the micrographs of Fig. 19 reveal that the surfaces of many voids are irregular, some with sharp angles. For such cavities, the internal field will not be uniform and the value of the cavity volume integral in (4) will deviate from that of the regular geometries examined. In addition, some of the cavities are in close proximity, particularly with solder layer (a). For these reasons, the calculated conductivity reduction factors should be considered as order of magnitude approximations. The visual appearance of the solder layers might suggest a more pronounced reduction of the thermal conductivity, particularly with layer (b). However, the volume ratios in the examined regions are at most 3.2%, causing a change of only 5% in the heat flow.

VI. CONCLUSION

Expressions for effective thermal conductivity of systems with spherical and spheroidal inclusions were derived from the general properties of Laplacian fields. These expressions are in good agreement with simulations for the spherical and spheroidal geometries considered, for small cavity dimensions and volume fraction. In the case of spherical cavities, the accuracy is within 1% for volume fractions less than approximately 0.1. Systems with multiple voids are treated by summation of the total cavity volume, with the inherent assumption that they are sufficiently small and sparse that their individual field disturbances do not significantly interact.

Based on estimates from the cross-sectional micrographs, the reduction in conductivity for the solder layer is at worst approximately 5% for the devices in this test group.

APPENDIX A

EFFECTIVE THERMAL CONDUCTIVITY FOR A VOLUME CONTAINING A VOID

With reference to Fig. 2, case 1 (denoted by suffix 1) refers to a uniform material of thermal conductivity σ_o and case 2 (suffix 2) to a material into which a void of volume v_c and thermal con-

ductivity σ_c has been introduced. The temperature and heat flow distributions change from T_1 and \mathbf{q}_1 to T_2 and \mathbf{q}_2 respectively while the boundary conditions are such that $T_1 = T_2$ on the surface S surrounding the volume $v_T = v_o + v_c$.

Consider the surface integral

$$\int_S (T_1 - T_2)(\mathbf{q}_2 - \mathbf{q}_1) \cdot d\mathbf{s} = 0. \quad (\text{A1})$$

This must be zero by definition through the specification $T_1 = T_2$ on the surface S . (A1) may be expressed as a volume integral

$$\int_{v_o+v_c} \nabla \cdot ((T_1 - T_2)(\mathbf{q}_2 - \mathbf{q}_1)) dv = 0. \quad (\text{A2})$$

By expanding the divergence term, (A2) may be written as

$$\int_{v_o+v_c} \nabla \cdot ((T_1 - T_2)(\mathbf{q}_2 - \mathbf{q}_1)) dv = \int_{v_o+v_c} \nabla \cdot (T_1 \mathbf{q}_2) - \nabla \cdot (T_2 \mathbf{q}_1) dv - \int_{v_o+v_c} \nabla \cdot (T_2 \mathbf{q}_2) - \nabla \cdot (T_1 \mathbf{q}_1) dv. \quad (\text{A3})$$

By noting that $\nabla T_2 = -\mathbf{p}_2$ and $\nabla T_1 = -\mathbf{p}_1$, and that $\nabla \cdot \mathbf{q}_1 = \nabla \cdot \mathbf{q}_2 = 0$ the second term on the RHS of (A3) becomes

$$\int_{v_o+v_c} \nabla \cdot (T_2 \mathbf{q}_2) - \nabla \cdot (T_1 \mathbf{q}_1) dv = - \int_{v_o+v_c} (\mathbf{p}_2 \cdot \mathbf{q}_2 - \mathbf{p}_1 \cdot \mathbf{q}_1) dv.$$

In a similar fashion the first term on the RHS of (A3) may be expressed as

$$\int_{v_o+v_c} \nabla \cdot (T_1 \mathbf{q}_2) - \nabla \cdot (T_2 \mathbf{q}_1) dv = - \int_{v_o+v_c} (\mathbf{p}_1 \cdot \mathbf{q}_2 - \mathbf{p}_2 \cdot \mathbf{q}_1) dv.$$

This may be split into two separate volume integrals over v_o and v_c

$$\int_{v_o+v_c} \nabla \cdot (T_1 \mathbf{q}_2) - \nabla \cdot (T_2 \mathbf{q}_1) dv = \int_{v_o} (\mathbf{p}_2 \cdot \mathbf{q}_1 - \mathbf{p}_1 \cdot \mathbf{q}_2) dv + \int_{v_c} (\mathbf{p}_2 \cdot \mathbf{q}_1 - \mathbf{p}_1 \cdot \mathbf{q}_2) dv. \quad (\text{A4})$$

Then, by noting that $\mathbf{q}_1 = \sigma_o \mathbf{p}_1$ and $\mathbf{q}_2 = \sigma_o \mathbf{p}_2$ in v_o , the first term on the RHS of (A4) is zero, leaving

$$\int_{v_o+v_c} \nabla \cdot (T_1 \mathbf{q}_2) - \nabla \cdot (T_2 \mathbf{q}_1) dv = \int_{v_c} (\mathbf{p}_2 \cdot \mathbf{q}_1 - \mathbf{p}_1 \cdot \mathbf{q}_2) dv.$$

Thus

$$\int_{v_c} (\mathbf{p}_2 \cdot \mathbf{q}_1 - \mathbf{p}_1 \cdot \mathbf{q}_2) dv = \int_{v_c+v_o} (\mathbf{p}_1 \cdot \mathbf{q}_1 - \mathbf{p}_2 \cdot \mathbf{q}_2) dv. \quad (\text{A5})$$

For case 1 $\mathbf{q}_1 = \sigma_o \mathbf{p}_1$ over v_c , whilst for case 2 $\mathbf{q}_2 = \sigma_c \mathbf{p}_2$ over v_c . (A5) may thus be written

$$\int_{v_c} (\sigma_o - \sigma_c) \mathbf{p}_2 \cdot \mathbf{p}_1 dv = \sigma_o \int_{v_c+v_o} \mathbf{p}_1^2 dv - \int_{v_c+v_o} \mathbf{p}_2 \cdot \mathbf{q}_2 dv. \quad (\text{A6})$$

Consider the case of a thin, uniform layer of semi-infinite extent and thickness d with its upper and lower surfaces held at tem-

peratures T_U and T_L , respectively. \mathbf{p}_1 is then a uniform field of strength

$$|\mathbf{p}_1| = \frac{T_U - T_L}{d}.$$

Following the introduction of a void the thermal field becomes altered locally to yield a nonuniform field distribution \mathbf{p}_2 . The effective thermal conductivity of the region including the void may be defined through the original field distribution \mathbf{p}_1 and modified distribution \mathbf{p}_2 as

$$\sigma_{\text{EFF}} = \frac{\int \mathbf{p}_2 \cdot \mathbf{q}_2 dv}{\mathbf{p}_1^2 (v_c + v_o)}. \quad (\text{A7})$$

Then, using (A6), the effective thermal conductivity may be written

$$\sigma_{\text{EFF}} = \sigma_o - (\sigma_o - \sigma_c) \frac{\int \mathbf{p}_2 \cdot \mathbf{p}_1 dv}{\mathbf{p}_1^2 (v_c + v_o)}. \quad (\text{A8})$$

APPENDIX B

THERMAL FIELD RESULTING FROM THE INTRODUCTION OF AN ELLIPSOIDAL CAVITY IN A UNIFORM FIELD DISTRIBUTION

The derivation is analogous to the solution for a dielectric ellipsoid placed in a parallel electric field, as described by Stratton [7].

The temperature distribution, T , arising from an ellipsoidal cavity is obtained from the superposition of the original undisturbed distribution, T_0 , and the distribution arising from the presence of the cavity, T_1

$$T = T_0 + T_1 \quad (\text{B1})$$

and for an initial uniform field

$$T_0 = -p_1 x. \quad (\text{B2})$$

A general ellipsoid, centred at the origin and with semi-principal axes of length a , b , c , can be written in terms of rectangular coordinates

$$\frac{x^2}{a^2} + \frac{y^2}{b^2} + \frac{z^2}{c^2} = 1. \quad (\text{B3})$$

It is convenient to work in terms of the ellipsoidal coordinates: u , v , w , which are related to the rectangular coordinates by

$$\begin{aligned} x &= \pm \sqrt{\frac{(u+a^2)(v+a^2)(w+a^2)}{(b^2-a^2)(c^2-a^2)}} \\ y &= \pm \sqrt{\frac{(u+b^2)(v+b^2)(w+b^2)}{(c^2-b^2)(a^2-b^2)}} \\ z &= \pm \sqrt{\frac{(u+c^2)(v+c^2)(w+c^2)}{(a^2-c^2)(b^2-c^2)}} \end{aligned} \quad (\text{B4})$$

and $u > -c^2$; $-c^2 > v > -b^2$; $-b^2 > w > -a^2$.

The surface of an ellipsoid is defined by $u = \text{constant}$. It is helpful to define

$$R_s = \sqrt{(s+a^2)(s+b^2)(s+c^2)} \quad s = u, v, w. \quad (\text{B5})$$

The Laplacian of a scalar, T , in ellipsoidal coordinates is

$$\begin{aligned} \nabla^2 T &= \frac{4}{(u-v)(v-w)(w-u)} \left[(v-w)R_u \frac{\partial}{\partial u} \left(R_u \frac{\partial T}{\partial u} \right) \right. \\ &\quad \left. + (w-u)R_v \frac{\partial}{\partial v} \left(R_v \frac{\partial T}{\partial v} \right) + (u-v)R_w \frac{\partial}{\partial w} \left(R_w \frac{\partial T}{\partial w} \right) \right]. \end{aligned} \quad (\text{B6})$$

Considering first the undisturbed temperature distribution defined by (B2). Substituting for x from (B4)

$$T_0 = -p_1 x = -p_1 \sqrt{\frac{(u+a^2)(v+a^2)(w+a^2)}{(b^2-a^2)(c^2-a^2)}} \quad (\text{B7})$$

which can be rewritten

$$\begin{aligned} T_0 &= C_1 F_1(u) F_2(v) F_3(w) \\ \text{where: } C_1 &= \frac{-p_1}{\sqrt{(b^2-a^2)(c^2-a^2)}}; \quad F_1 = \sqrt{(u+a^2)}; \\ F_2 &= \sqrt{(v+a^2)}; \quad F_3 = \sqrt{(w+a^2)}. \end{aligned} \quad (\text{B8})$$

Now consider the effect of introducing the cavity.

If the boundary conditions are to be satisfied, the temperature T_1 must vary over the surface of an ellipsoid ($u = \text{constant}$) in the same manner as T_0 , so the form of T_1 is

$$T_1 = C_2 G_1(u) F_2(v) F_3(w). \quad (\text{B9})$$

Now T_1 is a solution of Laplace's Equation in ellipsoidal coordinates, so substituting from (B6)

$$\begin{aligned} \nabla^2 T_1 &= 0 \\ \therefore \left[(v-w)R_u \frac{\partial}{\partial u} \left(R_u \frac{\partial T_1}{\partial u} \right) + (w-u)R_v \frac{\partial}{\partial v} \left(R_v \frac{\partial T_1}{\partial v} \right) \right. \\ &\quad \left. + (u-v)R_w \frac{\partial}{\partial w} \left(R_w \frac{\partial T_1}{\partial w} \right) \right] = 0. \end{aligned} \quad (\text{B10})$$

Substituting into (B10) from (B5), (B8), (B9), it can be shown that

$$R_u \frac{d}{du} \left(R_u \frac{dG_1}{du} \right) - G_1 \left\{ \frac{u}{2} + \frac{(b^2+c^2)}{4} \right\} = 0 \quad (\text{B11})$$

which can be expanded

$$\frac{d^2 G_1}{du^2} - \frac{1}{R_u} \frac{dR_u}{du} \frac{dG_1}{du} - \frac{1}{R_u^2} \left\{ \frac{u}{2} + \frac{(b^2+c^2)}{4} \right\} G_1 = 0. \quad (\text{B12})$$

(B12) is a second-order differential equation relating G_1 to the ellipsoidal variable, u . One solution is: $G_1 = F_1 = \sqrt{(u+a^2)}$.

If a general second-order differential equation

$$\frac{d^2 y}{dx^2} + p(x) \frac{dy}{dx} + q(x)y = 0$$

has a solution y_1 then a second independent solution y_2 is given by

$$y_2 = y_1 \int \frac{e^{-\int p \cdot dx}}{y_1^2} \cdot dx \quad (\text{B13})$$

Applying the result in (B13) to (B12) with $p = (1/R_u)(dR_u/du)$ and $y_1 = F_1 = \sqrt{(u+a^2)}$ gives

$$G_1 = F_1 \int \frac{du}{F_1^2 R_u}. \quad (\text{B14})$$

From (B8) and (B9)

$$T_1 = \frac{C_2 G_1}{C_1 F_1} T_0 \quad \text{and substituting from (B14) :}$$

$$T_1 = T_0 \frac{C_2}{C_1} \int \frac{du}{F_1^2 R_u} \quad (\text{B15})$$

so, the temperature distribution, T^+ , outside the ellipsoid can be written

$$T^+ = T_0 + T_1 = F_1(u)F_2(v)F_3(w)\{C_1 + C_2 A_1\} \quad (\text{B16})$$

where, for the ellipsoid with surface defined by $u = 0$

$$A_1 = \int_0^\infty \frac{du}{F_1^2 R_u} = \int_0^\infty \frac{du}{\sqrt{(u+a^2)^3(u+b^2)(u+c^2)}}. \quad (\text{B17})$$

For the temperature distribution, T^- , inside the ellipsoid, possible solutions are

$$T^- \propto F_1 F_2 F_3 \quad \text{or} \quad T^- \propto G_1 F_2 F_3$$

but G_1 is infinite at $u = -c^2$, whereas F_1 is finite at all points within $u = 0$, so

$$T^- = C_3 F_1(u)F_2(v)F_3(w). \quad (\text{B18})$$

The constants C_2 and C_3 must satisfy the boundary conditions on the ellipsoid surface at $u = 0$. First, the two temperature distributions must be equal at the surface

$$T^+|_{u=0} = T^-|_{u=0} \quad (\text{B19})$$

and substituting from (B16) and (B18)

$$\{C_1 + C_2 A_1\} = C_3. \quad (\text{B20})$$

The second boundary condition arises from the continuity of heat flow across the surface

$$\sigma \left[\frac{dT^+}{du} \right]_{u=0} = \sigma_c \left[\frac{dT^-}{du} \right]_{u=0} \quad (\text{B21})$$

which leads to

$$C_2 = \frac{abc}{2\sigma} (\sigma - \sigma_c) C_3. \quad (\text{B22})$$

From (B20) and (B22)

$$C_3 = \frac{C_1}{1 + \frac{abc}{2\sigma} (\sigma_c - \sigma) A_1} \quad (\text{B23})$$

and combining (B7), (B8), (B18), (B23), the temperature inside the ellipsoidal cavity is

$$T^- = \frac{-p_1 x}{1 + \frac{abc}{2\sigma} (\sigma_c - \sigma) A_1} \quad (\text{B24})$$

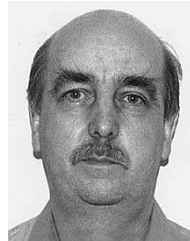
and the field distribution is

$$p_2 = \frac{p_1}{1 + \frac{abc}{2\sigma} (\sigma_c - \sigma) A_1}. \quad (\text{B25})$$

REFERENCES

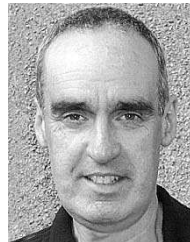
[1] Indium Corporation of America, Indalloy data.
 [2] L. S. Pritchard, C. M. Johnson, P. P. Acarnley, and A. B. Horsfall, "An investigation of the structural and thermal transfer characteristics of commercial power MOSFET devices using experimental and modeling techniques," in *Proc. IEE Int. Conf. Power Electronics, Machines and Drives*, 2002, pp. 562–567.

[3] G. R. Hadley, "Thermal conductivity of packed metal powders," *Int. J. Heat Mass Transfer*, vol. 29, no. 1, pp. 909–920, 1986.
 [4] D. Y. Tzou and J. Li, "Some scaling rules for the overall thermal conductivity in porous materials," *J. Composite Mater.*, vol. 29, no. 1, pp. 634–652, 1995.
 [5] L. S. Verma, A. K. Shrotriya, R. Singh, and D. R. Chaudhary, "Thermal conduction in two-phase materials with spherical and nonspherical inclusions," *J. Phys. D: Appl. Phys.*, no. 24, pp. 1729–1737, 1991.
 [6] J. P. Holman, *Heat Transfer*. New York: McGraw-Hill, 1992.
 [7] J. A. Stratton, *Electromagnetic Theory*, 1st ed. New York: McGraw-Hill, 1941.
 [8] ANSYS Incorporated, ANSYS 5.7.1, Cannonsburg, PA, 2003.



Leonard S. Pritchard received the Ph.D. degree in the effects of X-radiation on the electrical discharge properties of high voltage insulation from Sunderland University, Sunderland, U.K., in 1999.

From 1993 to 1999, he worked in the high voltage industry, where he was involved with electrical testing, discharge analysis and thermal modeling of polymers and resin processing. He moved to the Department of Electrical and Electronic Engineering, University of Manchester Institute of Science and Technology, Manchester, U.K., in 1999, investigating prebreakdown discharge activity over insulator surfaces. In 2001, he joined the Department of Electrical, Electronic and Computer Engineering, University of Newcastle upon Tyne, U.K., as part of a research group studying real time temperature estimation of power semiconductor devices.



Paul P. Acarnley received the B.Sc. and Ph.D. degrees in electrical engineering from Leeds University, Leeds, U.K., in 1974 and 1977, respectively, and the M.A. degree from Cambridge University, Cambridge, U.K., in 1978.

After seven years in the Department of Engineering, Cambridge University, he joined the Power Electronics, Drives and Machines Group, University of Newcastle upon Tyne, U.K., in 1986. His book *Stepping Motors: A Guide To Theory and Practice* (London, UK: IEE, 1982, 2002). In 2003, he founded Research Engineering Education Services (RESEEDS). He is also Research Consultant in the School of Engineering, Robert Gordon University, Aberdeen, and Emeritus Professor at the University of Newcastle upon Tyne. His principal research interest is in the control of electric drives, including work on state and parameter estimation. In addition, he has made contributions in the areas of stepping motors, permanent-magnet generators, flywheel energy storage, and brushless dc drives.

Dr. Acarnley is a Fellow of the Institution of Electrical Engineers.



C. Mark Johnson (S'89–M'91) received the B.A. degree in engineering and the Ph.D. degree in electrical engineering from the University of Cambridge, Cambridge, U.K., in 1986 and 1991, respectively.

From 1990 to 1992, he was a Research Associate at the University of Cambridge, investigating GTO thyristors for traction applications. In 1992, he was appointed Lecturer at the University of Newcastle, U.K., where his research included the design, analysis and characterization of power semiconductor devices, resonant power conversion, and instrumentation. From 1998 to 2001, he managed the U.K. National Programme on Silicon Carbide Electronics and in 2000 he became Reader of Power Electronics at the University of Newcastle. In 2003, he was appointed Research Professor of Power Electronic Systems in the Electrical Machines and Drives Research Group, University of Sheffield, U.K. He continues to research power semiconductor devices, power device packaging, power module technologies, and power electronic applications. His specialist interests include power electronics for hostile environments and the thermal and electromagnetic management of power electronic systems.